

A Three-dimensional simulation study of the performance of Carbon Nanotube Field Effect Transistors with doped reservoirs and realistic geometry

Gianluca Fiori¹, Giuseppe Iannaccone¹ and Gerhard Klimeck²

¹ Dipartimento di Ingegneria dell'Informazione, Università di Pisa, 56100 Pisa, Italy

² School of Electrical Engineering, Network for Computational Nanotechnology,

Purdue University, West Lafayette, IN USA.

email: g.fiori@iet.unipi.it, Tel. +39 050 2217639

Abstract

In this work, we simulate the expected device performance and the scaling perspectives of Carbon nanotube Field Effect Transistors (CNT-FETs), with doped source and drain extensions. The simulations are based on the self-consistent solution of the 3D Poisson-Schrödinger equation with open boundary conditions, within the Non-Equilibrium Green's Function formalism, where arbitrary gate geometry and device architecture can be considered. The investigation of short channel effects for different gate configurations and geometry parameters shows that double gate devices offer quasi ideal subthreshold slope and DIBL without extremely thin gate dielectrics. Exploration of devices with parallel CNTs show that On currents per unit width can be significantly larger than the silicon counterpart, while high-frequency performance is very promising.

Index Terms

Carbon nanotubes, Ballistic transport, NEGF, Technology CAD.

I. INTRODUCTION

Carbon nanotubes (CNTs) represent a promising alternative to conventional silicon technology [1] for future nanoelectronics at the end of the ITRS roadmap [2]. Since the first work on the topic by Iijima [3], significant improvements have been achieved, both from the point of view of technology and physical modeling. In particular, Heinze et al. [4] have demonstrated Schottky Barrier CNT FETs, where the modulation of the current is mainly determined by the field-induced modulation of the nanotube band structure at the CNT ends. Such a working principle, however, strongly limits device performance. The ambipolar behavior, the poor control of the channel,

and the possible degradation of electrical properties like I_{on}/I_{off} ratio, deeply affects such kind of devices, especially nanotubes with large diameters, as shown in [5]. To obtain acceptable Drain Induced Barrier Lowering (DIBL), it has been demonstrated that downscaling of device dimensions has to follow particular rules, like maintaining the ratio between the channel length and the oxide thickness larger than 18 [5].

To alleviate these problems different solutions have been proposed to achieve channel modulation of the barrier. Javey et al. [6] and Nosho et al. [7] have shown for example that ohmic contacts can be obtained by choosing Pd or Ca as metal for the contacts, respectively. Inducing charge in the source and drain regions is another possible solution, reported for example in [8] and in [9].

Channel modulation has also been obtained [10], [11] by the definition of multiple gates able to fix independent potentials both in the reservoirs and in the channel as well as transparent Schottky barrier at the contacts.

In a scenario where many geometries are feasible, adequate physical models and simulation tools are necessary not only to provide explanations to experimental results, but also to define device guidelines for the fabrication of CNT FETs, with performance benchmarked against their mainstream silicon counterpart.

Gate-all-around CNT FETs have been studied [13], [14] where the three-dimensional Poisson equation has been reduced to two dimensions because of the cylindrical symmetry of the electrostatic potential, and transport has been computed through the Landauer formalism. Such coaxial geometry has also been adopted in [15], where the Poisson equation has been coupled with the Non-Equilibrium Green's Function (NEGF) formalism, using a mode space approach, which enables the computation of transport to a small number of electron subbands with a small computational cost.

However, planar gate structures are more attractive because of their simpler fabrication technology, and all the experimental data discussed above are on planar geometries.

A full three-dimensional approach has been followed in [16], where the Poisson equation has been solved using the method of moments. Such a method provides the advantage of requiring the computation of the Poisson equation only in regions where charge is not zero, with the drawback that it is practically impossible to treat more than two different dielectric constants.

In this work, we focus on realistic and experimentally relevant CNT-FETs with doped source and drain extensions and evaluate their performance against the requirements at the end of the ITRS. To this purpose, we have developed a code able to solve the full band Schrödinger equations with open boundary conditions in the NEGF framework. Such a module has been included in our three-dimensional Poisson solver NANOTCAD *ViDES* [17], which can deal with very general structures, since it does not take advantage of particular symmetries, and can consider structures in which both CNTs and crystalline semiconductors are simultaneously present.

Our realistic simulations show that CNT-FETs are very attractive for *i)* their capabilities of suppressing short channel effects, *ii)* driving high On currents per unit length *iii)* their potential for THz applications, providing I_{on}/I_{off} ratio required by the ITRS for the 15 nm gate length, and *iv)* their potential for THz applications. On the other hand, we shall show that the subthreshold slope deteriorates for a gate voltage close to zero, due to filling of hole states in the channel.

II. SIMULATION APPROACH

The potential profile in the three-dimensional simulation domain obeys the Poisson equation

$$\begin{aligned} \nabla [\epsilon(\vec{r}) \nabla \phi(\vec{r})] = & -q [p(\vec{r}) - n(\vec{r}) + N_D^+(\vec{r}) \\ & - N_A^-(\vec{r}) + \rho_{fix}] , \end{aligned} \quad (1)$$

where $\phi(\vec{r})$ is the electrostatic potential, $\epsilon(\vec{r})$ is the dielectric constant, N_D^+ and N_A^- are the concentration of ionized donors and acceptors, respectively and ρ_{fix} is the fixed charge. The electron and hole concentration (n and p , respectively) are computed by solving the Schrödinger equation with open boundary conditions, by means of the NEGF formalism [18]. A tight-binding Hamiltonian with an atomistic (p_z orbitals) real space basis [19] has been used with a hopping parameter $t=2.7$ eV.

The Green's function can then be expressed as

$$G(E) = [EI - H - \Sigma_S - \Sigma_D]^{-1} , \quad (2)$$

where E is the energy, I the identity matrix, H the Hamiltonian of the CNT, and Σ_S and Σ_D are the self-energies of the source and drain, respectively. As can be seen, transport is here assumed to be completely ballistic.

The considered CNTs are all zig-zag nanotubes, but the proposed approach can be easily generalized to nanotubes with a generic chirality, since the required changes involve only the Hamiltonian matrix. Once the length and the chirality of the nanotube are defined, the coordinates in the three-dimensional domain of each carbon atom are computed [20]. After that, the three-dimensional domain is discretized so that a grid point is defined in correspondence of each atom, while a user specified grid is defined in regions not including the CNT.

A point charge approximation is assumed, i.e. all the free charge around each carbon atoms is spread with a uniform concentration in the elementary cell including the atom. In particular, the electron and hole densities are computed from the Density of States (DOS), derived by the NEGF formalism. Assuming that the chemical potential of the reservoirs are aligned at the equilibrium with the flat Fermi level of the CNT, and given that there are no fully confined states, the electron concentration is

$$\begin{aligned} n(\vec{r}) = & 2 \int_{E_i}^{+\infty} dE [\text{DOS}_S(E, \vec{r}) f(E - E_{F_S}) \\ & + \text{DOS}_D(E, \vec{r}) f(E - E_{F_D})] , \end{aligned} \quad (3)$$

while the hole concentration is

$$\begin{aligned} p(\vec{r}) = & 2 \int_{-\infty}^{E_i} dE \{ \text{DOS}_S(E, \vec{r}) [1 - f(E - E_{F_S})] \\ & + \text{DOS}_D(E, \vec{r}) [1 - f(E - E_{F_D})] \} , \end{aligned} \quad (4)$$

where f is the Fermi-Dirac occupation factor, and DOS_S (DOS_D) is the density of states injected by the source (drain), and E_{F_S} (E_{F_D}) is the Fermi level of the source (drain).

The current has been computed by means of the Landauer formula

$$I = \frac{2q}{h} \int_{-\infty}^{+\infty} dE T(E) [f(E - E_{F_S}) - f(E - E_{F_D})] , \quad (5)$$

where q is the electron charge, h is Planck's constant and $\mathcal{T}(E)$ is the transmission coefficient computed as

$$\mathcal{T} = -Tr \left[\left(\Sigma_S - \Sigma_S^\dagger \right) G \left(\Sigma_D - \Sigma_D^\dagger \right) G^\dagger \right], \quad (6)$$

where G is the Green's function, while Σ_S and Σ_D are the source and drain self-energy matrices [18]. The Green's function is computed by means of the Recursive Green's Function (RGF) technique [21], [22]. A particular attention must be put in the definition of each self-energy matrix, which can be interpreted as a boundary condition of the Schrödinger equation. In particular, in our simulation we have considered a self-energy for semi-infinite leads boundary conditions, which enables to consider the CNT as connected to infinitely long CNTs at its ends.

We have to point out that the computation of the self-energy is quite demanding. In order to achieve faster results, we have followed the approach proposed in [25], which provides results four times faster as compared to a simple under-relaxation method.

We have to point out that, using a real space basis, the computed current takes into account intra- and inter-band tunneling, since, as compared to the mode space approach, all the bands of the nanotube are considered simultaneously.

From a numerical point of view, the non-linear system has been solved with the Newton/Raphson (NR) method with the Gummel iterative scheme. In particular, the Schrödinger equation is solved at the beginning of each NR cycle of the Poisson equation, and the charge density in the CNT is kept constant until the NR cycle converges (i.e. the correction on the potential is smaller than a predetermined value). The algorithm is then repeated cyclically until the norm of the difference between the potential computed at the end of two subsequent NR cycles is smaller than a predetermined value.

Some convergence problems however may be encountered using this iterative scheme. Indeed, since the electron density is independent of the potential within a NR cycle, the Jacobian is null for points of the domain including carbon atoms, losing control over the potential correction. We have then tried, according with the predictor/corrector scheme proposed by Trellakis et al. [23] to find a suitable expression for the charge predictor, in order to give an approximate expression for the Jacobian at each step of the NR cycle. To this purpose, we have used an exponential function for the predictor, also found independently by Polizzi et al. [24]. In particular, if n is the electron density as in (3), the electron density n_i at the i -th step of the NR cycle can be expressed as

$$n_i = n \exp \left(\frac{\phi_i - \tilde{\phi}}{K_B T} \right), \quad (7)$$

where $\tilde{\phi}$ and ϕ_i are the electrostatic potential computed at the first and i -th step of the NR cycle, respectively, while K_B and T are the Boltzmann constant and the temperature. Same considerations follow for the hole concentration. Since the electron density n is extremely sensitive to small changes of the electrostatic potential between two NR cycles, the exponential function acts in the overall procedure as a dumping factor for charge variations. In this way, convergence has been improved especially in the subthreshold regime as well as in the strong inversion regime. Problems however are still present for example in regions of the device where the charge

in the nanotube is not compensated by fixed charge, like in the case of bound states in the channel, where the right-hand term of the Poisson equation is considerably large.

III. RESULTS AND DISCUSSIONS

First, we consider a (11,0) CNT embedded in SiO₂, with a diameter d of 0.9 nm, an undoped channel of varying length L and n-doped CNT extensions of 10 nm at the source and drain ends (Fig. 1). The CNT extensions have a stoichiometric ratio f of fully ionized donors.

As a first attempt to study CNT-FET performance, we have considered the impact of the molar fraction f on the current in the off-state regime. Fig. 2 shows the current for $V_{DS} = 0.5$ V and $V_{GS} = 0$ V as a function of f , for two double gate (DG) CNT-FETs with $t_{ox}=2$ nm, and $L=7$ nm and 15 nm. As can be seen, for the $L=7$ nm device the current is extremely sensitive to f , and a small variation in the number of ionized atoms in the source and drain extensions can determine variations of the current of almost two orders of magnitude. However, as the channel length is increased, such effect is weakened, since the field generated by uncompensated donors in the reservoirs is less effective in lowering the channel barrier as the channel length is increased.

Since the number of donors is of the order of tens, current dispersion due to random dopant fluctuations can be problematic as shown in Fig. 2, where the current for a $L=7$ nm (7,0) CNT is shown. In this case, the number of atoms in the reservoirs has been decreased by a factor of $\frac{11}{7}$ and the current in the off states varies in this case by almost three orders of magnitude for the same range of doping factor.

For DC properties, we evaluate the devices in terms of short channel effects, I_{on} and I_{off} currents. We first consider short channel effects for different gate layouts (single, double and triple gate) for the same channel length $L = 15$ nm (Fig. 3).

The subthreshold swing S and DIBL as a function of the oxide thickness are plotted in Figs. 4a and 4b. Null Neumann boundary conditions are imposed on the lateral faces of the transversal cross sections, in order to consider an array of CNTs. As expected, the more gates surround the channel, the better is channel control. Triple gate devices show an ideal behavior even for the thickest oxide we have considered (5 nm), while quasi-ideal S is obtained for the double gate structure in the whole considered range of SiO₂ thickness. A single gate provides acceptable S and DIBL for 2 nm oxides. Fig. 5 shows the S and DIBL as a function of the channel length for a DG device with oxide thickness t_{ox} of 1 and 2 nm. DG devices show both very good S and DIBL down to 10 nm, and still acceptable values at 7 nm, while smaller channel lengths suffer from excessive degradation of the gate voltage control over the channel.

From here on, we will focus on a double gate structure, with $t_{ox}=2$ nm and the cross section shown in Fig 3b. Fig. 6a shows the on-current I_{on} per unit width defined as the current obtained for $V_{GS} = V_{DS} = 0.8$ V, as a function of the channel length, assuming a lateral dielectric separating adjacent nanotubes of 2 nm. In Fig. 6b, I_{on} is plotted as a function of the nanotube diameter, for a device with channel length equal to 7 nm.

Short channel effects become more important, as the channel length is decreased, and at the same biasing conditions shorter devices show larger I_{on} currents, since lowering of the channel barrier occurs. Moreover, as far

as the CNT diameter is increased, quantized states along each atom ring are closer in energy so that more subbands participate to electron transport, increasing channel conductance.

In Fig. 7a we show the On current as a function of the normalized tube density per unit length $\rho = d/T$, where T is the distance between the center of two nanotubes, as illustrated in the inset of Fig. 7a. All the results show that CNT-FETs can drive significant currents. As compared to the ITRS requirements, in the case of the most densely packed array, the current per unit length is almost 7 times larger than that expected for high performance devices at the 32 nm technology node (hp32 : effective gate length equal to 13 nm), and 6 times for the 22 nm technology node (hp22 : effective gate length equal to 9 nm).

The off-current (I_{off}), defined as the current obtained for $V_{GS} = 0$ V and $V_{DS} = 0.8$ V, is 15 times larger than that required both for the hp32 and hp22 nodes (Fig. 7b). However, as shown in Fig. 8a, where the Off-current as a function of the normalized tube density is depicted, as the density decreases also the current in the off-state decreases, so that for tube density smaller than 8×10^{-2} we obtain a I_{on}/I_{off} ratio larger than that required by the ITRS for the hp32 (Fig. 8b).

As observed also in [26], the degradation of the off-current is due to the presence of bound states in the valence band, which, for high doping and for large drain-to-source voltages are occupied by holes tunneling from the drain reservoir (Fig. 9a). For smaller V_{DS} , bound states are quite far from the drain Fermi level (Fig. 9b), so the linear behavior in the semilog plot of the transfer characteristics in the subthreshold regime is almost recovered, as shown in Fig. 10.

Another interesting effect due to the bound states, is that in the negative gate voltage regime, when band-to-band tunneling occurs at both source and drain ends, the current increases for negative gate voltage (Fig. 11). For larger V_{DS} , this effect requires higher V_{GS} in order to be observed, since the larger the drain-to-source voltage, the stronger the influence of the bound states in the valence band, which act against the activation of band-to-band tunneling process. In addition, as can be seen in the case of $V_{DS}=0.1$ V, for negative gate voltages, resonant states appear. Since in the considered CNTs the band gap is close to 1 eV, the above considerations suggest that such effect could also limit the performance of silicon devices in the decananometer regime.

Fig. 12 shows the transconductance g_m as a function of the gate voltage for devices with channel length of 5 nm, 7 nm and 10 nm computed for $V_{DS} = 0.8$ V. The transconductance peaks are in correspondence of the gate voltage at which the first one-dimensional subband crosses the source Fermi level. As can be seen, good values of the transconductance are obtained for the all three considered devices.

We now focus our attention on switching and high-frequency performance of CNTs. The typical figure of merit for digital applications is the intrinsic device speed, defined as $\tau = C_G V_{DD} / I_{on}$, where V_{DD} is the supplied voltage and C_G is the differential gate capacitance for $V_{GS} = 0.8$ V (Fig. 13a). This quantity is typically used to estimate the time it takes an inverter to switch, when its output drives another inverter, represented as a load capacitance C_G , as shown in the inset of Fig. 13a. Compared to the ITRS requirements for the hp22 technology node, the obtained τ are at least 12 times faster.

CNT-FETs also show good potential for THz applications [27]. In Fig. 13b, the cut-off frequency defined as

$f_T = \frac{g_m}{2\pi C_G}$ is shown as a function of the channel length : f_T is of the order of tens of THz, and the values obtained by simulations are larger than those found in [27], where the gate capacitance is overestimated. As a word of caution, we must consider that additional stray capacitances could reduce the estimated f_T and τ .

CONCLUSION

We have developed a novel 3D NEGF-based simulation tool for arbitrary CNT-FET architectures, which has enabled us to investigate the performance perspectives of CNT-FETs from an engineering point of view.

We have in principle demonstrated that random distribution of dopants in the reservoirs can significantly affect device performance, and degrade current in the off-state by several orders of magnitude. We have shown that double-gate structures exhibit very small short channel effects even with rather thick silicon oxide gate dielectric (5 nm), and still acceptable subthreshold swing and Drain Induced Barrier Lowering for devices with channel length down to 7 nm.

The driving currents and the transconductance are very good as compared to the ITRS requirements, while the I_{off} may pose some problems due to the presence of localized hole states in the channel. However, good I_{on}/I_{off} can be achieved reducing the tube density in the CNT-FET array, still satisfying ITRS requirements.

We have also shown the double gate CNT-FETs are very promising for THz applications if stray capacitances can be maintained under control.

ACKNOWLEDGMENT

Support from the EU SINANO NoE (contract no. 506844), from the MIUR-PRIN “Architectures and models for nanoMOSFETs” is gratefully acknowledged, and NSF grant # EEC-0228390.

REFERENCES

- [1] R. Martel, HSP Wong, K. Chan, and P. Avouris, "Carbon nanotube field-effect transistors for logic applications", in *IEDM Tech. Dig.*, 2001, pp. 159-162.
- [2] International Technology Roadmap for Semiconductor 2004 update. Available : <http://public.itrs.net>.
- [3] S. Iijima, "Helical microtubules of graphite carbon", *Nature*, Vol. 354, pp. 56-58, Nov. 1991.
- [4] S. Heinze, J. Tersoff, R. Martel, V. Derycke, J. Appenzeller, and Ph. Avouris, "Carbon nanotubes as schottky barrier transistors", *Phys. Rev. Lett.*, Vol. 89, pp. 106801-106803, Aug. 2002.
- [5] J. Appenzeller, J. Knoch, R. Martel, V. Derycke, S. Wind, and P. Avouris, "Short-channel like effects in schottky barrier carbon nanotube field-effect transistors", in *IEDM Tech. Digest*, 2002, pp. 285-288.
- [6] A. Javey, J. Guo, Q. Wang, M. Lundstrom, and H. Dai, "Ballistic carbon nanotube field-effect transistors", *Nature*, Vol. 424, pp. 654-657, Aug. 2003.
- [7] Y. Noshu, Y. Ohno, S. Kishimoto, and T. Mizutani, "n-type carbon nanotube field-effect transistors fabricated by using Ca contact electrodes" *Appl. Phys. Lett.*, Vol. 86, p. 073105, Feb. 2005.
- [8] J. Chen, C. Klinke, A. Afzali, and P. Avouris, "Self-aligned carbon nanotube transistors with charge transfer doping", *Appl. Phys. Lett.*, Vol. 86, p.123108, Mar. 2005.
- [9] M Bockrath, J. Hone, A. Zettl, P. McEuen, A. G. Rinzler, and R. E. Smalley, "Chemical doping of individual semiconducting carbon-nanotube ropes", *Phys. Rev. B*, Vol. 61, pp. R10607-R10608, Apr. 2000.
- [10] S. J. Wind, J. Appenzeller, and P. Avouris, "Lateral scaling in carbon-nanotube field-effect transistors", *Phys. Rev. Lett.*, Vol. 91, pp. 58301, Aug. 2003.
- [11] Yu-Ming Lin, J. Appenzeller, J. Knoch, and P. Avouris, "Novel carbon nanotube fet design with tunable polarity", in *IEDM Tech. Digest*, 2004, pp. 29.2.1-29.2.4.
- [12] E. Ungersbock, A. Gehring, H. Kosina, S. Selberherr, B. Cehong, and W. B. Choi, . "Simulation of carrier transport in carbon nanotube field effect transistor", in *ESSDERC*, 2003, pp. 411-414.
- [13] J. P. Clifford, L. C. Castro, and D. L. Pulfrey, "Electrostatic of partially gated carbon nanotube fets", *IEEE Trans. on Nanotechnology*, Vol. 3, pp. 281-286, Jun. 2004.
- [14] J. Clifford, D. L. John, and D. L. Pulfrey, "Bipolar conduction and drain-induced barrier thinning in carbon nanotube fets", *IEEE Trans. on Nanotechnology*, Vol. 2, pp. 181-185, Sept. 2003.
- [15] J. Guo, S. Datta, and M. Lundstrom, "A numerical study of scaling issue for schottky-barrier carbon nanotube transistors", *IEEE Trans. on Electr. Dev.*, Vol. 51, pp.172-177, Feb. 2004.
- [16] J. Guo, S. Datta, M. Lundstrom, and M. P. Anantram, "Towards multi-scale modeling of carbon nanotube transistors", Available at : <http://arxiv.org/abs/cond-mat/0312551>.
- [17] G. Fiori, G. Iannaccone "Code for the 3D Simulation of Nanoscale Semiconductor Devices, Including Drift-Diffusion and Ballistic Transport in 1D and 2D Subbands, and 3D Tunneling", *Journal of Computational Electronics*, Vol. 4, pp. 63-66, Sept. 2005.
- [18] S. Datta. "Nanoscale device modeling : Green's function method", *Superlattice and Microstructures*, Vol. 28, pp. 253-277, Jul. 2000.
- [19] J. Guo et al. "Performance analysis and design optimization of near ballistic carbon nanotube field-effect transistors", in *IEDM Tech. Digest*, 2004, pp. 703-706.
- [20] R. Saito, G. Dresselhaus, and M. S. Dresselhaus, *Physical Properties of carbon nanotubes*. Imperial college Press, London, England, 2003, pp.35-58.
- [21] R. Lake, G. Klimeck, R. C. Bowen, and D. Jovanovic, "Single and Multi-band modeling of quantum electron transport through layered semiconductors devices", *J. Appl. Phys.*, Vol. 81, pp.7845-7869, Feb. 1997.
- [22] A. Svizhenko, M. P. Anantram, T. R. Govindam, and B. Biegel, "Two-dimensional quantum mechanical modeling of nanotransistors", *J. Appl. Phys.*, Vol. 91, pp. 2343-2354, Nov. 2001.
- [23] A. Trellakis, A. T. Galick, A. Pacelli, and U. Ravaioli, "Iteration scheme for the solution of the two-dimensional Schrödinger-Poisson equations in quantum structures", *J. Appl. Phys.*, Vol. 81, pp. 7880-7884, Mar. 1997.
- [24] E. Polizzi, and N. B. Abdallah, "Subband decomposition approach for the simulation of quantum electron transport in nanostructures", *J. Comp. Phys.*, Vol. 202, pp. 150-180, Aug. 2005.

- [25] M. P. Lopez Sancho, J. M. Lopez Sancho, and J. Rubio, "Highly convergent schemes for the calculation of bulk and surface green function", *J. Phys. F.*, Vol. 15, pp. 851-858, Oct. 1984.
- [26] J. Knoch, S. Mantl, and J. Appenzeller, "Comparison of transport properties in carbon nanotube field-effect transistor with Schottky contacts and doped source/drain contacts", *Solid-State Electr.*, Vol. 49, pp.73-76, Aug. 2005.
- [27] P.J. Burke, "AC performance of nanoelectronics : towards a ballistic THz nanotube transistor", *Solid-State Electr.*, Vol. 48, pp.1981-1986, Jun. 2004.

Fig. 1. Three-dimensional structure of the simulated CNT-FETs.

Fig. 2. Current density for $V_{DS} = 0.5$ V and $V_{GS} = 0$ V as a function of the molar fraction of doping atoms f for Double Gate (11,0) CNT-FETs with $L=7$ nm and $L=15$ nm and (7,0) $L=7$ nm DG CNT-FET.

Fig. 3. Transversal cross section of the CNT-FETs with different gate structures : a) single gate; b) double gate; c) triple gate. Null Neumann boundary condition are imposed on lateral ungated surfaces.

Fig. 4. a) Subthreshold slope and b) Drain Induced Barrier Lowering as a function of the oxide thickness, for $L=15$ nm and for different gate layouts. $f = 10^{-3}$.

Fig. 5. a) Subthreshold slope and b) Drain Induced Barrier Lowering as a function of the channel length, for the DG CNT-FETs with $t_{ox}=2$ nm and $t_{ox}=1$ nm .

Fig. 6. a) On Current per unit width as a function of the channel length for a double gate CNT-FET (2 nm lateral dielectric between adjacent nanotubes); b) I_{on} current per nanotube as a function of the nanotube diameter, for a $L=7$ nm double gate CNT-FET. $t_{ox} = 2$ nm, $f = 5 \times 10^{-3}$.

Fig. 7. a) On current as a function of the nanotube normalized density per unit length $\rho = d/T$ for a double gate CNT-FET with $L=15$ nm; b) Off-current as a function of the channel length for a double gate CNT-FET.

Fig. 8. a) Off-current as a function of the nanotube normalized density per unit length $\rho = d/T$ for a double gate CNT-FET with $L=15$ nm; b) I_{on}/I_{off} ratio as a function of the nanotube normalized density per unit length $\rho = d/T$ for a double gate CNT-FET with $L=15$ nm.

Fig. 9. Density of states computed for the device with $L=7$ nm, for $V_{GS} = 0$ V and a) $V_{DS} = 0.8$ V, b) $V_{DS} = 0.5$ V as a function of the energy and the coordinate along the nanotube axis. Dashed lines are in correspondence of the source and drain Fermi level.

Fig. 10. Transfer characteristics for the double gate CNT-FET with $L=7$ nm, for $V_{DS} = 0.5$ V and $V_{DS} = 0.8$ V; $t_{ox} = 2$ nm, $f = 5 \times 10^{-3}$.

Fig. 11. Transfer characteristics for the double gate CNT-FET with $L=7$ nm, for $V_{DS} = 0.5$ V and $V_{DS} = 0.1$ V; $t_{ox} = 1$ nm, $f = 5 \times 10^{-3}$.

Fig. 12. Transconductance as a function of the gate voltage for double gate CNT-FETs with different channel lengths : $L=5$ nm, 7 nm and 10 nm; $t_{ox} = 2$ nm, $V_{DS} = 0.8$ V, and $f = 5 \times 10^{-3}$.

Fig. 13. a) Inverse of the intrinsic device speed, defined as $\tau = C_G V_{DD} / I_{on}$ as a function of the channel length for double gate CNT-FET; $V_{DD} = 0.8$ V, C_G is the gate capacitance. b) Cut-off frequency as a function of the gate length, for the double gate CNT-FET. $t_{ox} = 2$ nm, $f = 5 \times 10^{-3}$.

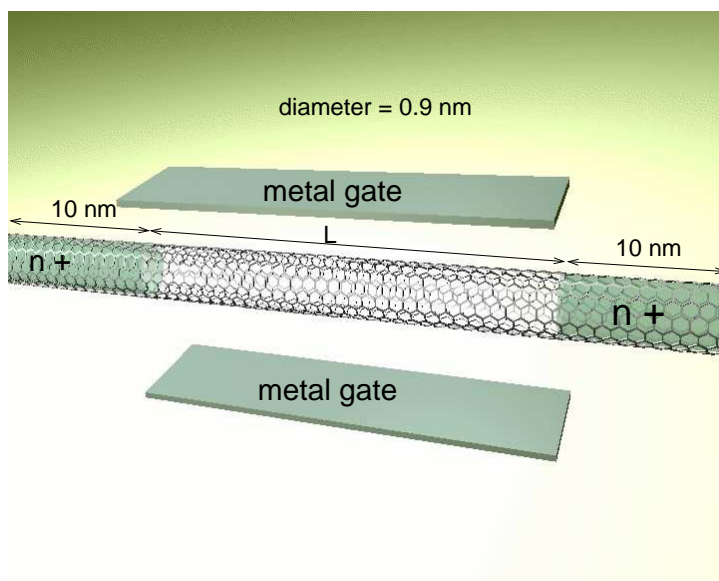


FIG. 1

Gianluca Fiori et al.

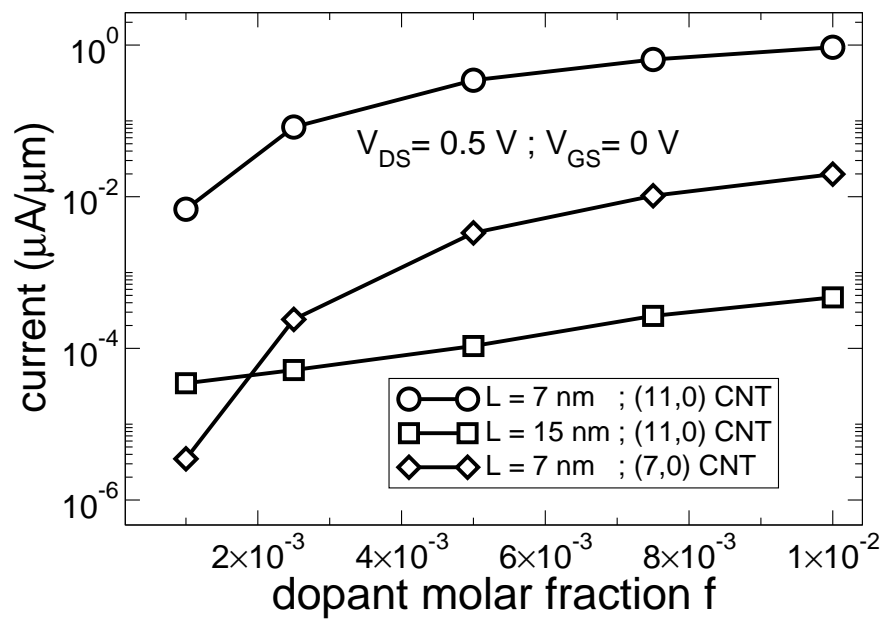


FIG. 2

Gianluca Fiori et al.

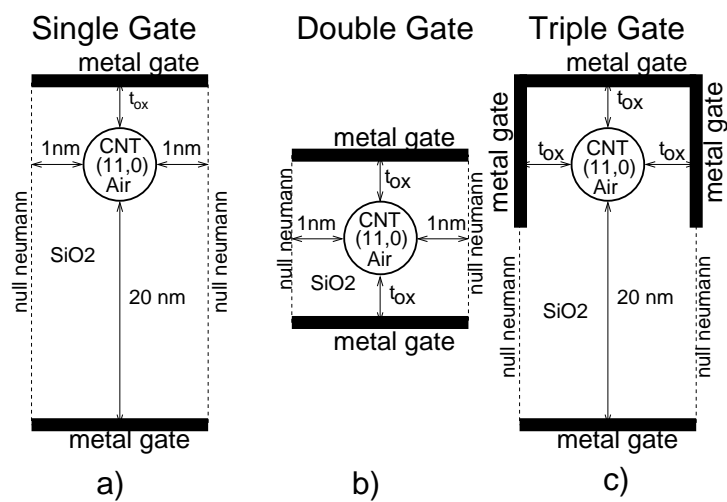


FIG. 3

Gianluca Fiori et al.

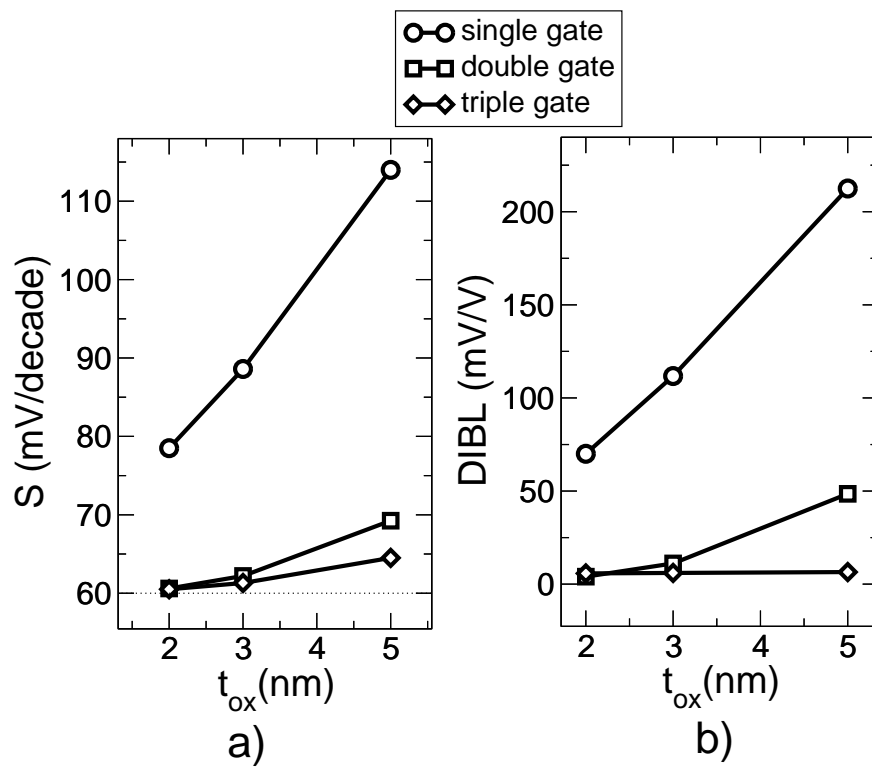


FIG. 4

Gianluca Fiori et al.

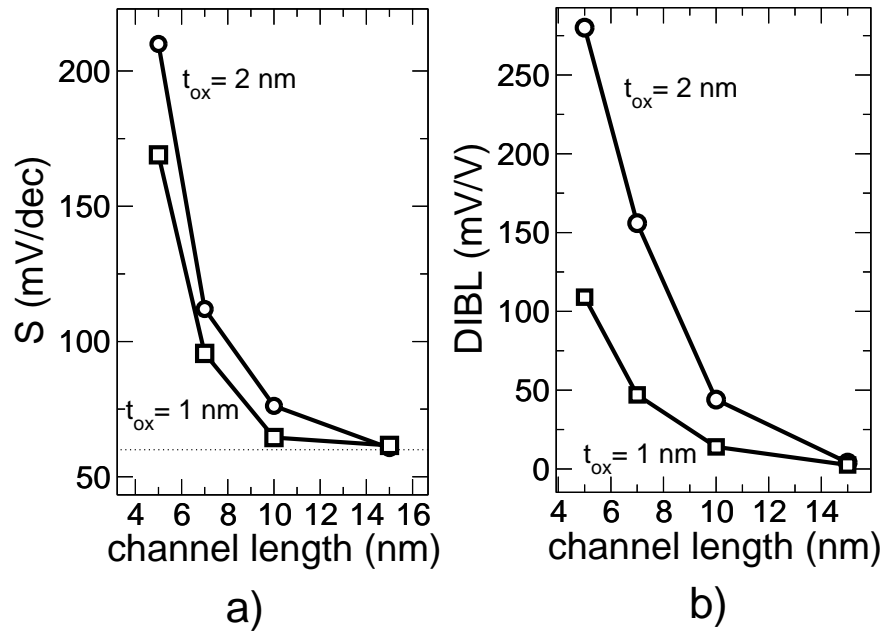


FIG. 5

Gianluca Fiori et al.

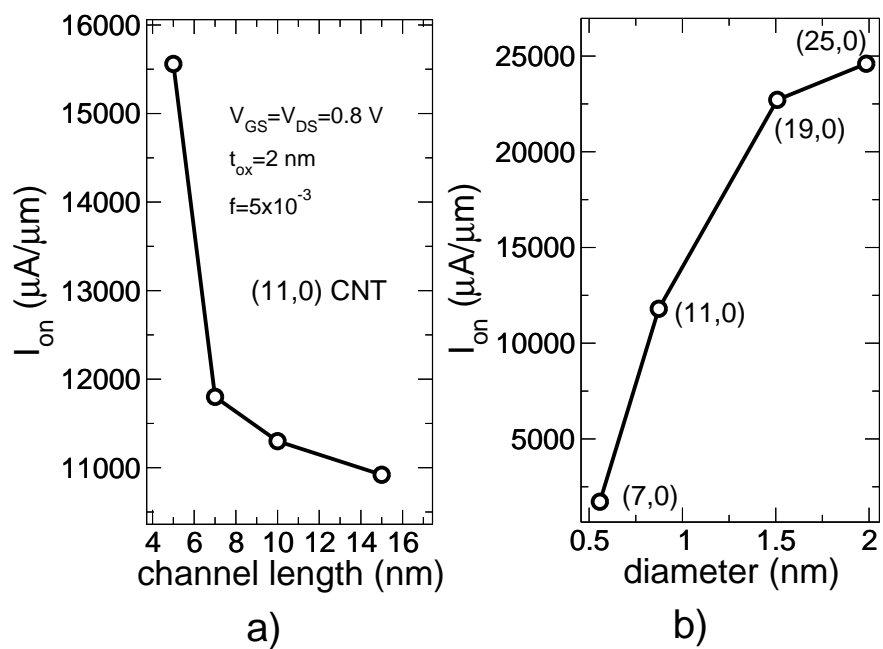


FIG. 6

Gianluca Fiori et al.

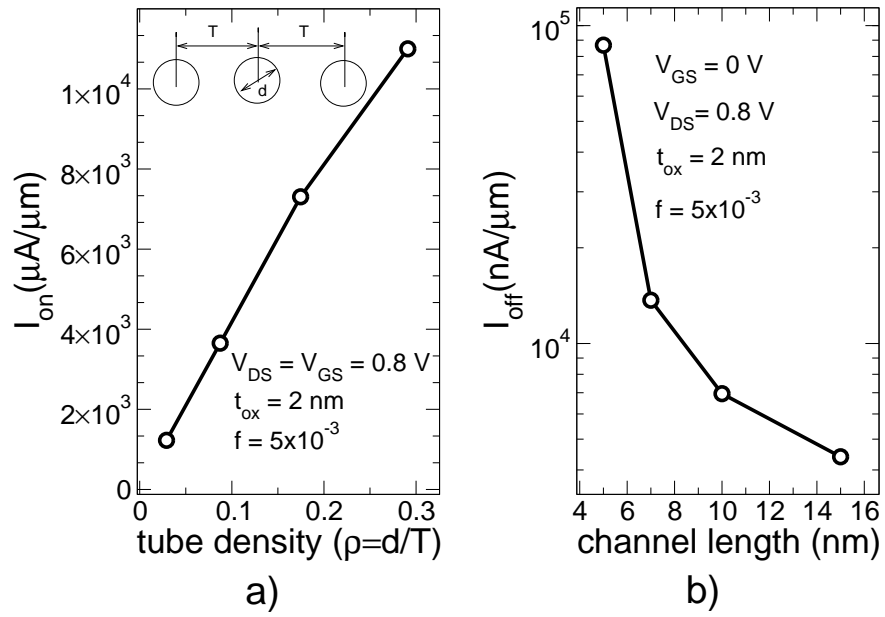


FIG. 7

Gianluca Fiori et al.

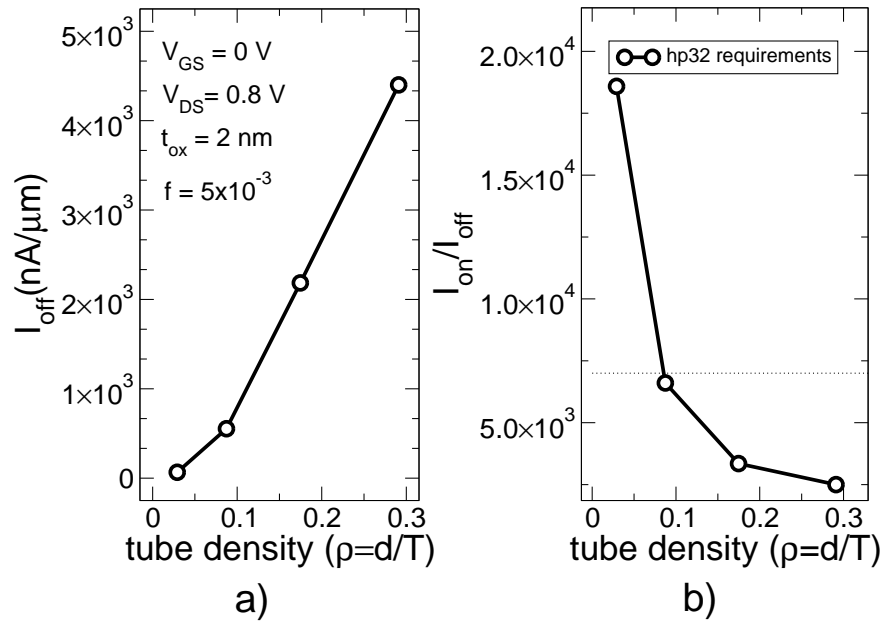
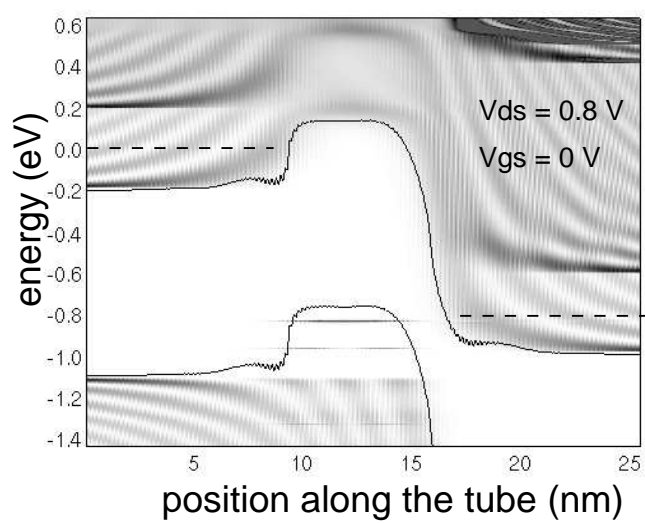
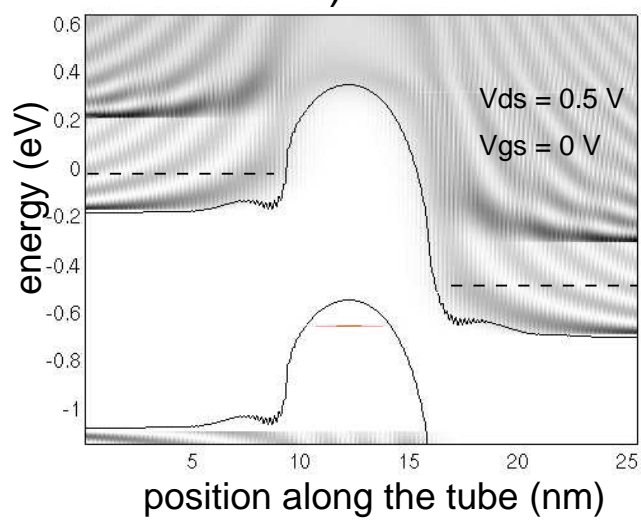


FIG. 8

Gianluca Fiori et al.



a)



b)

FIG. 9

Gianluca Fiori et al.

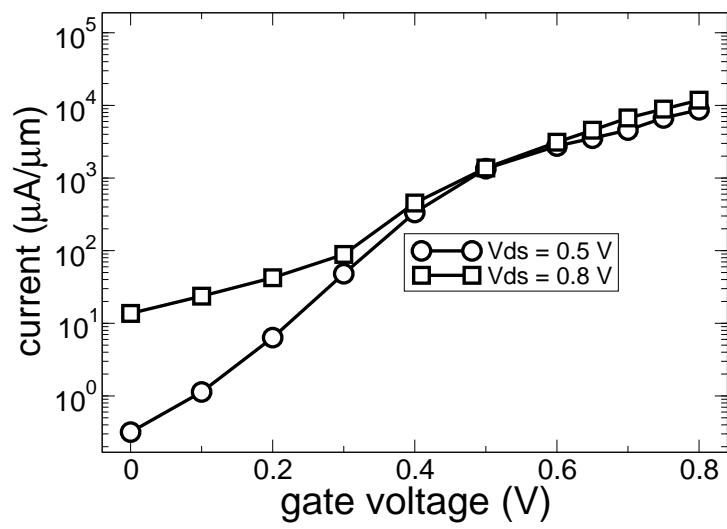


FIG. 10

Gianluca Fiori et al.

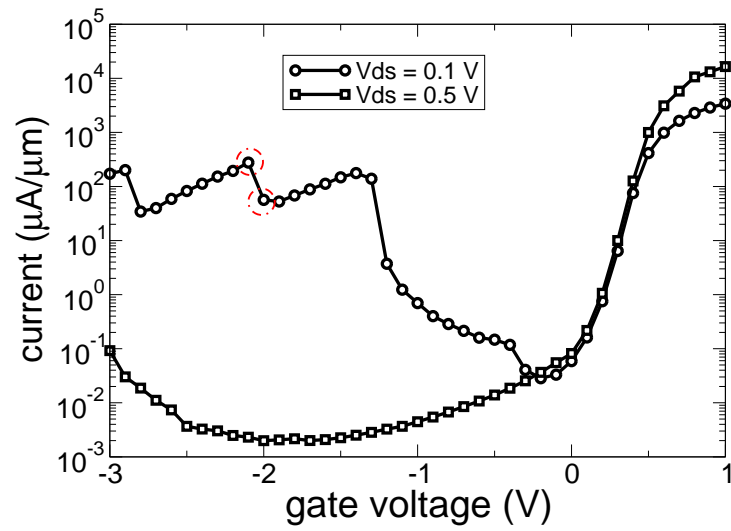


FIG. 11

Gianluca Fiori et al.

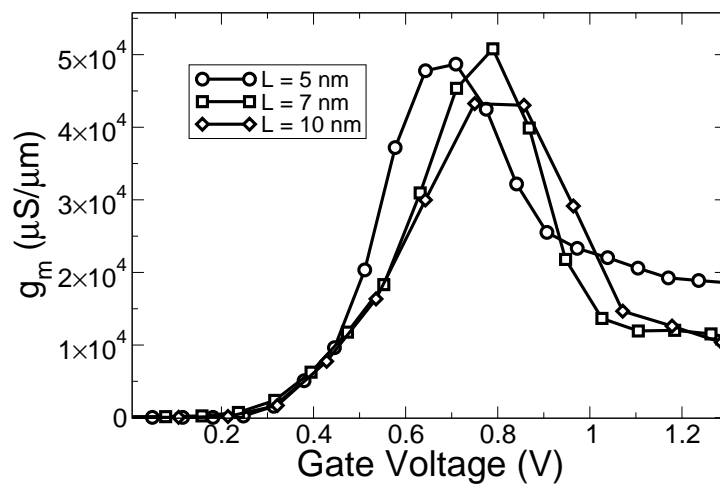


FIG. 12

Gianluca Fiori et al.

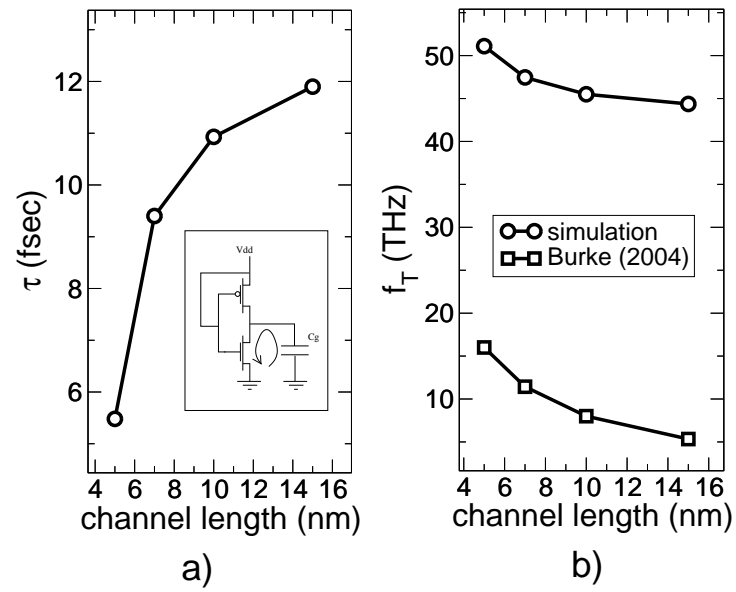


FIG. 13

Gianluca Fiori et al.